

doi: [10.12097/gbc.2024.01.015](https://doi.org/10.12097/gbc.2024.01.015)

南天山造山带东段变流纹岩原岩的喷发时代与构造背景:来自锆石U-Pb年龄和微量元素的约束

黄少英^{1,2}, 陈守文^{3,4*}, 袁文芳^{1,2}, 罗彩明^{1,2}, 段云江^{1,2}, 亢茜^{1,2}, 章凤奇^{3,4}
HUANG Shaoying^{1,2}, CHEN Shouwen^{3,4*}, YUAN Wenfang^{1,2}, LUO Caiming^{1,2},
DUAN Yunjiang^{1,2}, KANG Qian^{1,2}, ZHANG Fengqi^{3,4}

1. 中国石油天然气集团有限公司超深层复杂油气藏勘探开发技术研发中心,新疆库尔勒841000;

2. 中国石油天然气集团有限公司天然气成藏与开发重点实验室,新疆库尔勒841000;

3. 浙江大学地球科学学院,浙江杭州310058;

4. 教育部含油气盆地构造研究中心,浙江杭州310058

1. *Exploration and Development Center of Ultra-Deep Complex Oil and Gas Reservoirs, China National Petroleum Corporation, Korla 841000, Xinjiang, China;*

2. *Key Laboratory of Gas Reservoir Formation and Development, China National Petroleum Corporation, Korla 841000, Xinjiang, China;*

3. *School of Earth Sciences, Zhejiang University, Hangzhou 310058, Zhejiang, China;*

4. *Structural Research Center of Oil & Gas Bearing Basin of Ministry of Education, Hangzhou 310058, Zhejiang, China*

摘要:【研究目的】变质岩的组成和时代是认识造山带基底性质和形成演化的重要窗口。通过南天山造山带东段的哈满沟地区辛格尔组中变流纹岩的时代和锆石微量元素研究,探讨变流纹岩的时代及其对南天山构造演化的意义。【研究方法】系统开展南天山造山带东段的哈满沟地区辛格尔组中变流纹岩岩相学、LA-ICP-MS锆石U-Pb定年和锆石微量元素分析,并结合区域研究成果,对南天山造山带的构造背景开展综合研究。【研究结果】LA-ICP-MS锆石U-Pb定年结果表明,变流纹岩原岩形成于早泥盆世(418~412 Ma)。锆石轻稀土元素相对亏损,重稀土元素相对富集,显示负Eu异常、正Ce异常的特征。微量元素显示U、Hf正异常,Nb、La、Pr、Ti负异常。根据锆石微量元素分析,推测流纹岩喷发时的地壳厚度小于35 km,且其岩浆源区存在斜长石分离结晶作用,锆石Ti温度计指示其岩浆结晶温度较高(>800°C),属于高温岩浆成因,提出该流纹岩的发育可能与大陆裂谷作用有关。【结论】结合前人研究,推测南天山造山带早古生代可能是塔里木克拉通的一部分,其北缘为活动大陆边缘,大致在晚志留世—早泥盆世受北缘俯冲后撤作用影响,南天山地区经历了强烈的弧后伸展,本次识别的流纹岩可能形成于早泥盆世弧后伸展裂谷的构造背景。

关键词:南天山造山带;变流纹岩;锆石U-Pb年龄;泥盆纪;高温岩浆作用;弧后伸展

创新点:南天山造山带东段的哈满沟地区辛格尔组中变流纹岩形成于早泥盆世,并非前人研究认为的太古宙地层,南天山造山带东段早泥盆世发育弧后伸展裂谷。

中图分类号:P597.3 **文献标志码:**A **文章编号:**1671-2552(2025)02/03-0424-17

Huang S Y, Chen S W, Yuan W F, Luo C M, Duan Y J, Kang Q, Zhang F Q. The eruptive age and tectonic setting of the protolith of the meta-rhyolite in the eastern segment of the South Tianshan Orogenic Belt: Constraints from zircon U-Pb age and trace elements. *Geological Bulletin of China*, 2025, 44(2/3): 424–440

收稿日期: 2024-01-11; 修订日期: 2024-04-15

资助项目:国家自然科学基金面上项目《塔里木板块西南部青白口纪晚期盆地属性与转换过程及其对超大陆聚合的制约》(批准号:42372244)

作者简介:黄少英(1977-),男,博士,高级工程师,从事盆地基础地质研究。E-mail: huangsyy-tlm@petrochina.com

*通信作者:陈守文(1995-),男,博士,从事构造地质学研究。E-mail: csw_0916@163.com

Abstract: [Objective] The composition and age of metamorphic rocks provide a crucial window into understanding the nature, formation, and evolution of orogenic belt basements. Based on an analysis of zircon age and trace elements from the Xingeer Formation in the eastern part of the South Tianshan Orogenic Belt, this paper explores the age of meta-rhyolite and its significance for the tectonic evolution of the Southern Tianshan orogenic belt. [Methods] The lithology, LA-ICP-MS zircon U-Pb dating, and zircon trace element analysis of the meta-rhyolite in the Xingeer Formation, located in the eastern part of the South Tianshan Orogenic Belt, have been systematically conducted. The data have been comprehensively analyzed in conjunction with regional research findings. [Results] LA-ICP-MS zircon U-Pb dating results indicate that the protolith was formed in the Early Devonian (418~412 Ma). The zircon exhibits a relative depletion in light rare earth elements (LREE) and enrichment in heavy rare earth elements (HREE), characterized by a negative Eu anomaly and a positive Ce anomaly. Trace element analysis reveals positive anomalies of U and Hf, along with negative anomalies of Nb, La, Pr, and Ti. Based on zircon trace element analysis, it is inferred that the crustal thickness at the time of rhyolite eruption was less than 35 km, with evidence of plagioclase fractionation and crystallization in the magmatic source region. The zircon Ti thermometer indicates a high magmatic crystallization temperature ($>800^{\circ}\text{C}$), suggesting a high-temperature magmatic origin. This implies that the rhyolite's development may be associated with continental rifting. [Conclusions] Based on previous studies, it is inferred that the South Tianshan Orogenic Belt may have been part of the Tarim Craton during the Early Paleozoic, with its northern margin representing an active continental margin. Influenced by subduction and retreat along the northern margin, the South Tianshan region experienced significant back-arc extension during the Late Silurian to Early Devonian. The meta-rhyolite identified in this study is likely to have formed within the tectonic setting of Early Devonian back-arc extensional rifting.

Key words: South Tianshan Orogenic Belt; meta-rhyolite; zircon U-Pb age; Devonian; high temperature magmatism; back-arc extension

Highlights: In the eastern segment of the South Tianshan orogenic belt, the meso-rhyolite of the Xingeer Formation in the Hamangou area was formed during the Early Devonian, rather than in the Archean, as previously believed. During the Early Devonian, a back-arc extensional rift valley developed in the eastern part of the South Tianshan Orogenic Belt.

南天山造山带位于塔里木克拉通和伊犁-中天山地块之间,是古生代南天山洋俯冲消减及伊犁-中天山地块与塔里木克拉通北缘碰撞造山的产物([Jahn et al., 2004; Windley et al., 2007; Xiao et al., 2009, 2015; 刘桂萍等, 2020](#))。该造山带经历了南天山洋盆开启、扩张、俯冲、关闭等多期构造演化过程,保存了丰富的构造-岩浆-地层记录,为认识区域构造演化、板块作用历史、地壳增生等地质过程提供了重要线索([李曰俊等, 2009; Xiao et al., 2014; 刘桂萍等, 2020](#))。准确揭示造山带岩石组成和时代,是认识和恢复造山带构造演化历史的基础。造山带内的变质岩是阐明造山带基底性质、构造属性和演化的关键对象。南天山造山带内部发育多套变质岩系,区域地质调查显示,在库尔勒北部南天山造山带南缘出露一套太古宇辛格尔组,其岩性主要是一套以片岩为主夹少量变流纹岩的浅变质岩石。它是否是南天山造山带最古老的基底,一直缺乏可靠的同位素年龄约束。本次研究在野外地质调查的基础上,对哈满沟附近出露的辛格尔组与片岩呈互层发育的一套变流纹岩夹层开展了锆石U-Pb年代学研究,试图厘定变火山岩原岩的形成时代,结合锆石微量元素特

征和邻区构造-岩浆事件,探讨该流纹岩形成的构造背景,为南天山造山带演化提供地质限定。

1 地质背景和样品采集

1.1 地质背景

天山造山带位于中亚造山带西南部([图 1-a](#)),自东向西被分为东天山和西天山,其中,西天山主要由北天山增生造山带、中天山地块、伊犁地块和南天山造山带构成,其中,南天山造山带位于中天山地块与塔里木克拉通之间,北部与中天山地块的界线为中天山南缘断裂,南部与塔里木克拉通的界线为塔里木北缘断裂([高俊等, 2009; Han et al., 2015, 2016; Huang et al., 2018, 2020; 刘桂萍等, 2020, 2021; 图 1-b](#))。南天山造山带是一个大型增生杂岩体,岩石组成复杂,不仅发育前寒武纪基底岩石,古生代沉积地层,还发育有高压—超高压变质岩、蛇绿岩、岛弧火山岩和花岗岩等([Han et al., 2015, 2016; Huang et al., 2018, 2020; 于新慧等, 2020](#))。南天山造山带记录了古生代南天山洋从俯冲到消亡的历史,其形成和演化过程与伊犁-中天山地块和塔里木克拉通碰撞造山过程关系密切([Lin et al., 2013; Xiao and Santosh, 2014](#);

Han et al., 2015, 2016; Huang et al., 2018, 2020; 于新慧等, 2020; 王博等, 2022; Ning et al., 2023)。

南天山构造带岩石地层组成较复杂。总体上, 前寒武纪基底岩石出露有限, 主要包括古元古界木扎尔特群和兴地塔格群, 以及中元古界阿克苏群, 其中木扎尔特群出露于造山带西段的黑英山地区, 兴地塔格群和阿克苏群出露于造山带中段。在造山带东段库米什地区还出露角闪岩相的片麻岩、片岩、混合岩及混合花岗岩(Yang et al., 2009; 于新慧等, 2020)。古生代沉积盖层以陆源碎屑岩和碳酸盐岩为主, 其沉积时代主要为晚志留世—石炭纪。高压—超高压变质岩主要分布于阿克牙孜变质带, 记录了 320~310 Ma 的晚石炭世变质事件(Klemd et al., 2011, 2015; Han and Zhao, 2018; 刘桂萍等, 2020)。蛇绿岩主要出露在南天山构造带南部, 如米斯布拉克、柯尔腾柯斯河上游、满大勒克、库勒湖、色日克牙依拉克等地, 其形成时代为志留纪—泥盆纪早期(杨经绥等, 2010; Jiang et al., 2014, 2015; 刘桂萍等, 2020)。此外, 南天山造山带内广泛发育古生代岩浆活动, 岩石类型以花岗质侵入岩为主, 也有少量辉长岩、闪长岩, 岩浆活动时代主要为晚志留世—中泥盆世和晚石炭世—中二叠世 2 个阶段(朱志新等, 2008; Han et al., 2015; 图 2-a), 西段与中段晚石炭世—早二叠世侵入岩发育普遍, 东段则早古生代侵入岩和火山岩均有发育(Konopelko et al., 2007, 2009; Wang et al., 2011; Ge et al., 2012; Lin et al., 2013; 郭瑞清等, 2013; Zhao et al., 2015)。

1.2 样品采集

本次采集的变流纹岩样品位于南天山构造带东段的哈满沟地区, 距离南部库尔勒市区约 10 km。该地区的岩石地层单元包括辛格尔组、艾肯布拉克组和古生代侵入体(图 2-b)。前人研究认为, 辛格尔组属于兴地塔格群, 可能代表卷入了南天山造山带的太古宙基底岩系, 发育大理岩和黑云母片岩, 以及少量绢云母石英片岩, 被上覆侏罗系砂砾岩角度不整合覆盖(新疆维吾尔自治区地质局, 1959)。本次通过野外地质调查, 在辛格尔组(中亚组)中新识别出一套典型的变火山岩, 火山岩整体颜色较深, 面理发育, 指示浅变质特征(图 3)。

样品(HMG10)为深灰色变流纹岩。岩石具有明显的流纹构造和斑状结构。斑晶矿物主要为长石和石英。长石斑晶含量约为 30%, 半自形粒状, 以碱性

长石为主, 部分长石蚀变成绿帘石或绢云母。石英斑晶含量约为 10%, 半自形粒状, 大多发生动态重结晶亚颗粒化。基质为霏细结构, 主要为长英质矿物。可见磁铁矿、锆石等副矿物(图 3-a, b)。

样品(HMG12)同样为深灰色变流纹岩。岩石发育流纹构造和斑状结构。斑晶为长石和石英。长石斑晶含量约为 20%, 半自形粒状, 以斜长石为主, 部分长石蚀变成绢云母。石英斑晶含量约为 10%, 半自形粒状, 大多发生动态重结晶亚颗粒化。基质为霏细结构, 主要为长英质矿物。副矿物主要为磁铁矿、锆石等(图 3-c, d)。

2 分析方法

样品普通岩石薄片的制备、锆石分选和测年制靶及阴极发光(CL)照相工作均由廊坊诚信地质服务有限公司完成。锆石分选采用常规重液分离方法, 先将锆石等重矿物分选出来, 然后利用电磁分选将锆石等非磁性矿物分离, 在双目镜下通过手工挑选获得锆石颗粒。为避免人为对锆石矿物筛选的影响, 在分选过程中不考虑锆石颜色、粒度、自形程度等特征, 并将锆石颗粒固定在树脂上制成样品靶。采用砂纸和抛光机打磨抛光样品靶面, 使靶面的锆石内部结构充分暴露。利用扫描电镜拍摄 CL 图像, 获取锆石的结晶形态及内部结构信息。

锆石微量元素(含稀土元素)分析和 U-Pb 同位素定年在北京快科赛默科技有限公司完成。激光剥蚀系统为 New Wave NWR 193^{UC}, 电感耦合等离子体质谱仪(ICP-MS)为 Agilent 8900。激光剥蚀过程中采用高纯氦气作载气, 流速为 700 mL/min。激光采样为单点剥蚀, 实验使用激光束斑为 20 μm, 频率为 5 Hz, 能量密度为 3.5 J/cm²(李同宇等, 2022)。测试分析前, 利用 NIST SRM610 标样调谐使仪器的各项指标正常。分析期间, 锆石 U-Pb 同位素定年中采用 91500 标准锆石作外标进行同位素分馏校正, 用 Plešovice 锆石作为质量监控样。测试结束后, 使用数据处理软件 Iolite 进行离线数据处理(Paton et al., 2010)。该数据处理软件由澳大利亚墨尔本大学同位素研究组开发, 不仅优化了剥蚀孔下分馏模型, 同时可调用激光日志文件, 使数据处理更快捷与专业。获得数据后, 锆石 U-Pb 年龄的谐和图绘制和年龄加权平均值计算均采用 Isoplot 4.15 完成。

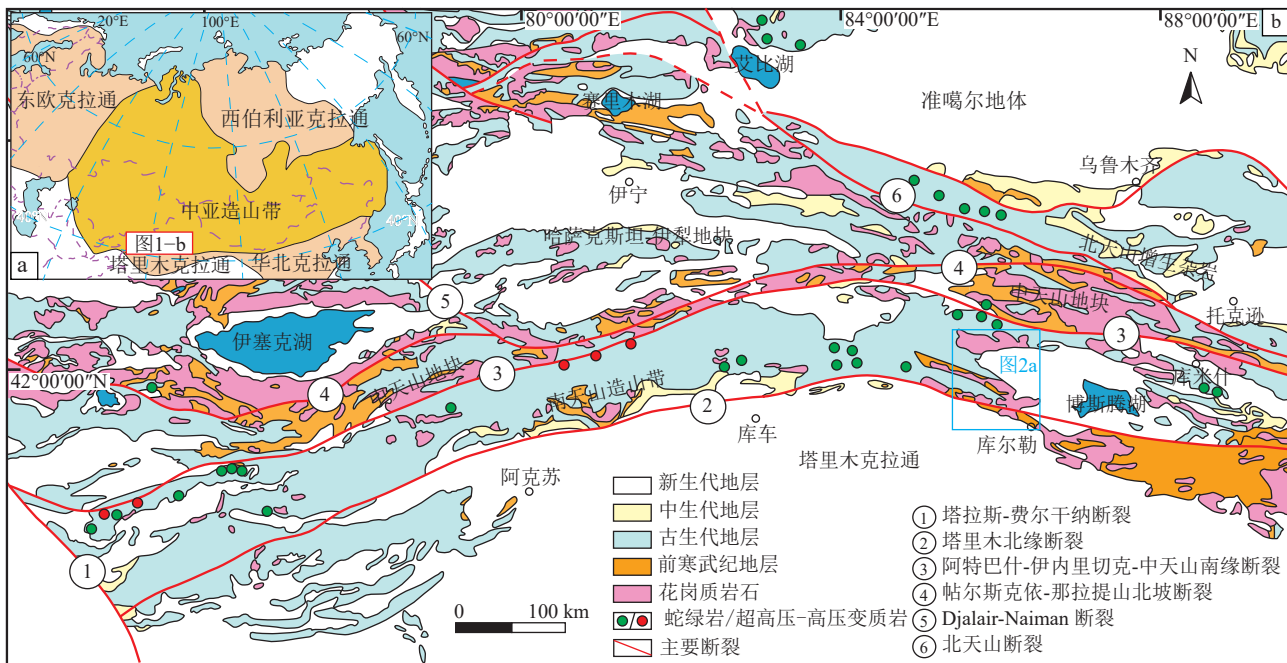


图1 中亚造山带及邻近克拉通分布简图(a, 据 Windley et al., 2007 修改)和南天山造山带及邻区大地构造简图(b, 据 Wang et al., 2018a 修改)

Fig. 1 Simplified map of the Central Asian Orogenic Belt and its adjacent cratons (a) and simplified geological map of the Southern Tianshan Orogenic Belt and its adjacent areas (b)

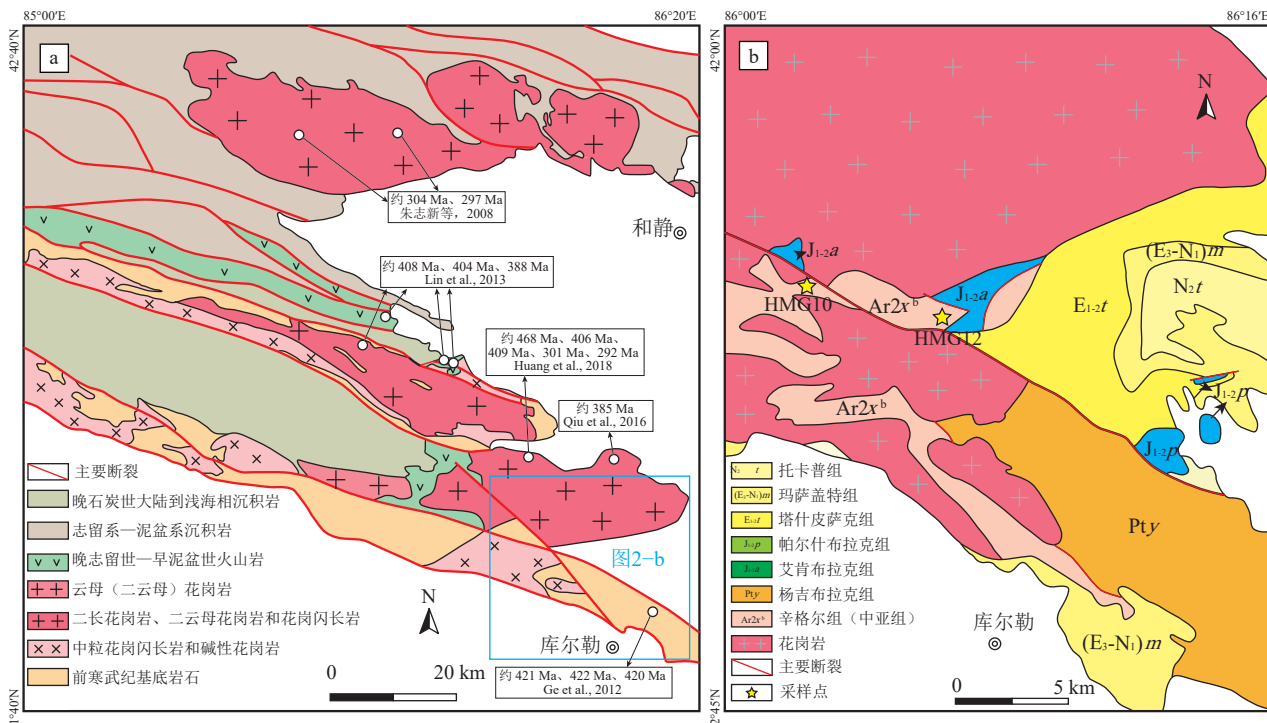


图2 库尔勒北部南天山造山带地质简图(a, 据 Lin et al., 2013 修改)和南天山造山带哈满沟地区地质简图(b, 据 新疆维吾尔自治区地质局, 1959 修改)

Fig. 2 Simplified geological map of South Tianshan Orogenic Belt in the northern Korla (a) and simplified geological map of the Hamangou region in the South Tianshan Orogenic Belt (b)

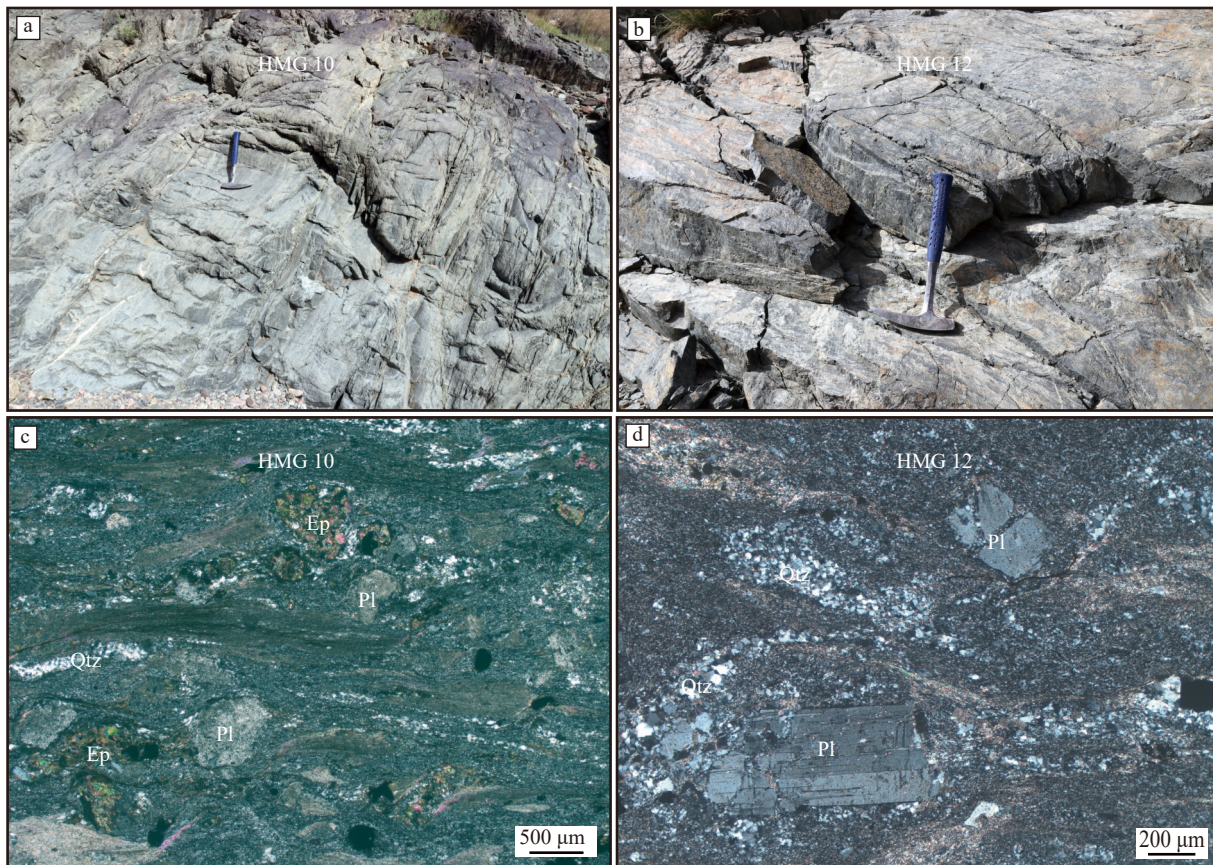


图 3 南天山造山带哈满沟地区变流纹岩野外和显微镜下照片

Fig. 3 Field and microscopic photos of the meta-rhyolites from the Hamangou area in the South Tianshan Orogenic Belt

a, b—变流纹岩野外露头, 显示弱变形特征; c, d—变流纹岩镜下照片, 发育流纹构造, 斑晶主要为长石。

Pl—斜长石; Qtz—石英; Ep—绿帘石

3 分析结果

基于上述分析方法, 本次研究对南天山构造带哈满沟地区辛格尔组的变流纹岩开展了锆石年代学和微量元素测试。锆石 U-Pb 同位素测年、微量和稀土元素测试结果分别见表 1 和表 2。

3.1 锆石 U-Pb 年龄

HMG10 变流纹岩样品中的锆石颗粒多呈自形柱状, 长 50~150 μm , 宽 50~80 μm , 长宽比为 1.5 : 1~2 : 1。锆石 CL 图像显示, 锆石内部发育振荡环带, 部分锆石包裹体较发育或具有裂纹(图 4-a)。锆石 Th 含量为 474×10^{-6} ~ 36.6×10^{-6} , U 含量为 393×10^{-6} ~ 45×10^{-6} , Th/U 值介于 0.76~1.39 之间(图 5-a), 表明这些锆石为岩浆成因(吴元保和郑永飞, 2004; 雷玮琰等, 2013)。随机选取 30 颗锆石进行 U-Pb 同位素、微量和稀土元素分析, 所有测试点都位于锆石边部具有振荡环带且没有裂

缝或包裹体发育的区域。分析结果显示, 30 个测试点的年龄数据均落在谐和线上, 表现出较高的谐和性(谐和度 >90%), $^{206}\text{Pb}/^{238}\text{U}$ 年龄值主要介于 462~394 Ma 之间, 除 23 号测试点(462 ± 10 Ma)年龄值偏大外, 其余 29 个测试点年龄值相对集中, 其年龄加权平均值为 412.4 ± 4.3 Ma(MSWD=2.3)(图 6-a, b), 代表了变流纹岩原岩岩浆冷却结晶的时间。

HMG12 变流纹岩样品中的锆石颗粒也具有自形柱状特点, 长 50~100 μm , 宽 30~50 μm , 长宽比为 1 : 1~1.5 : 1。锆石 CL 图像显示, 锆石内部同样具有清晰的岩浆振荡环带结构, 部分锆石可见少量包裹体或裂纹(图 4-a)。锆石 Th 含量为 699×10^{-6} ~ 89×10^{-6} , U 含量为 296×10^{-6} ~ 86×10^{-6} , Th/U 值介于 2.73~1.03 之间, 显示这些锆石同样具有岩浆成因锆石的特征(吴元保和郑永飞, 2004; 雷玮琰等, 2013)。随机选取 29 颗锆石进行 U-Pb 同位素、微量和稀土元素分析, 所有测试点均位于显示振荡环

表1 哈满沟变流纹岩 LA-ICP-MS 锆石 U-Th-Pb 同位素组成

Table 1 LA-ICP-MS zircon U-Th-Pb isotopic composition of metarhyolite from Hamangou

测点号	含量/ 10^{-6}			同位素比值						同位素年龄/Ma					
	Th	U	Th/U	$^{207}\text{Pb}/^{206}\text{Pb}$	1 σ	$^{207}\text{Pb}/^{235}\text{U}$	1 σ	$^{206}\text{Pb}/^{238}\text{U}$	1 σ	$^{207}\text{Pb}/^{206}\text{Pb}$	1 σ	$^{207}\text{Pb}/^{235}\text{U}$	1 σ	$^{206}\text{Pb}/^{238}\text{U}$	1 σ
HMG10															
01	49.5	50.3	0.98	0.0551	0.0066	0.509	0.06	0.0672	0.0023	240	240	406	40	419	14
02	66.7	61.6	1.08	0.0521	0.0058	0.478	0.05	0.0679	0.003	170	210	395	36	423	18
03	59.4	61.9	0.96	0.0528	0.0057	0.465	0.047	0.0655	0.0028	190	210	386	34	408	17
04	56.1	53.9	1.04	0.0572	0.0067	0.532	0.065	0.0662	0.0035	360	250	418	44	413	21
05	53.3	54.9	0.97	0.0563	0.0059	0.517	0.052	0.066	0.0029	350	220	414	35	412	17
06	47.3	59.5	0.79	0.052	0.01	0.452	0.08	0.0637	0.0037	160	360	367	54	398	22
07	218	157	1.39	0.0579	0.0043	0.525	0.038	0.0666	0.0019	430	150	429	26	415	11
08	66.2	64.4	1.03	0.0597	0.0066	0.518	0.056	0.063	0.0025	430	230	414	38	394	15
09	36.6	46	0.80	0.059	0.0077	0.521	0.064	0.0654	0.0028	340	260	412	42	408	17
10	87	74.1	1.17	0.0557	0.0058	0.511	0.048	0.0668	0.0028	330	210	411	31	416	17
11	36.7	45	0.82	0.0568	0.0068	0.498	0.056	0.0648	0.0028	300	240	399	38	404	17
12	58	70.6	0.82	0.0571	0.0063	0.521	0.06	0.0641	0.0024	370	220	414	39	401	15
13	53.2	53.5	0.99	0.0538	0.0069	0.485	0.059	0.0656	0.0022	190	240	389	40	410	13
14	68.8	69.6	0.99	0.0592	0.0088	0.521	0.069	0.0676	0.0039	430	300	432	55	421	24
15	52.6	53.9	0.98	0.0551	0.0073	0.472	0.06	0.0635	0.0022	270	260	381	40	397	13
16	41.6	45.8	0.91	0.0607	0.0076	0.567	0.078	0.0666	0.0032	440	260	440	51	415	19
17	73.6	61.4	1.20	0.0607	0.0096	0.542	0.084	0.0643	0.0034	470	330	430	56	401	20
18	58.9	57	1.03	0.062	0.0067	0.57	0.055	0.0688	0.0029	500	220	456	38	429	18
19	70.8	72	0.98	0.0578	0.0052	0.523	0.046	0.0656	0.0022	400	190	420	31	410	13
20	72.1	61	1.18	0.0511	0.0047	0.472	0.046	0.0665	0.0025	160	180	385	31	415	15
21	57.1	60.8	0.94	0.0562	0.0052	0.503	0.049	0.0646	0.0027	340	190	405	33	403	16
22	205	270	0.76	0.0548	0.0025	0.532	0.025	0.0699	0.0015	363	98	431	17	435.5	8.7
23	474	393	1.21	0.0557	0.0022	0.577	0.022	0.0743	0.0017	421	91	461	14	462	10
24	85.9	75.1	1.14	0.0561	0.0055	0.504	0.052	0.0648	0.0028	370	210	412	36	404	17
25	93.5	70.4	1.33	0.0591	0.0066	0.537	0.06	0.0659	0.0022	400	230	425	39	411	13
26	74.5	63.5	1.17	0.0514	0.0055	0.497	0.053	0.0688	0.0025	190	220	400	36	428	15
27	56.9	57.6	0.99	0.0557	0.0064	0.495	0.054	0.0655	0.0027	280	230	398	36	409	17
28	79	79.2	1.00	0.0539	0.0061	0.479	0.052	0.0648	0.0025	220	230	387	36	405	15
29	63	64.2	0.98	0.0585	0.0062	0.524	0.052	0.0651	0.0022	390	220	418	35	406	14
30	45.7	49.5	0.92	0.0574	0.0071	0.506	0.058	0.0646	0.0025	380	260	405	40	404	15
HMG12															
01	297	183	1.62	0.0575	0.0041	0.53	0.037	0.067	0.0019	430	160	427	25	418	11
02	163	120	1.36	0.055	0.0049	0.503	0.042	0.0669	0.0022	300	180	408	28	417	13
03	197	142	1.39	0.0697	0.0046	0.694	0.056	0.0684	0.0023	920	160	533	35	427	14
04	111	94.5	1.17	0.077	0.01	0.74	0.11	0.0675	0.0027	930	250	538	60	421	16
05	158	135	1.17	0.0566	0.0039	0.53	0.038	0.0678	0.0022	400	140	427	25	423	14
06	318	209	1.52	0.0529	0.0037	0.493	0.038	0.0661	0.0018	290	150	402	25	412	11
07	127	87	1.46	0.0584	0.0058	0.528	0.052	0.066	0.0027	400	200	422	34	412	16
08	297	200	1.49	0.0561	0.0026	0.527	0.028	0.0679	0.0021	410	100	427	18	423	13
09	465	256	1.82	0.0554	0.0034	0.501	0.028	0.0662	0.0017	360	130	413	20	413	10
10	223	166	1.34	0.0562	0.0042	0.524	0.041	0.0669	0.0016	370	160	422	27	417	10

续表 1

测点号	含量/ 10^{-6}				同位素比值						同位素年龄/Ma					
	Th	U	Th/U		$^{207}\text{Pb}/^{206}\text{Pb}$	1σ	$^{207}\text{Pb}/^{235}\text{U}$	1σ	$^{206}\text{Pb}/^{238}\text{U}$	1σ	$^{207}\text{Pb}/^{206}\text{Pb}$	1σ	$^{207}\text{Pb}/^{235}\text{U}$	1σ	$^{206}\text{Pb}/^{238}\text{U}$	1σ
11	213	116	1.84	0.0571	0.0044	0.53	0.044	0.0672	0.0023	400	160	426	28	419	14	
12	89	86.3	1.03	0.0526	0.0049	0.47	0.037	0.0658	0.0023	240	180	386	26	411	14	
13	324	221	1.47	0.0562	0.0032	0.516	0.03	0.0662	0.0015	400	130	419	20	413	9	
14	381	198	1.92	0.0603	0.0052	0.563	0.051	0.0678	0.0028	530	190	449	33	423	17	
15	245	189	1.30	0.0531	0.0038	0.478	0.032	0.0663	0.0021	260	150	397	23	413	12	
16	289	180	1.61	0.0556	0.0042	0.508	0.037	0.0659	0.0018	350	150	413	25	411	11	
17	214	126.4	1.69	0.057	0.0048	0.531	0.045	0.0676	0.0024	380	170	426	29	422	15	
18	312	183	1.70	0.0548	0.0037	0.505	0.034	0.0666	0.002	330	140	411	23	415	12	
19	683	250	2.73	0.053	0.0033	0.489	0.028	0.0674	0.0021	270	130	402	19	420	12	
20	404	245	1.65	0.0555	0.0033	0.538	0.034	0.07	0.0019	370	130	434	22	436	11	
21	239	160	1.49	0.0556	0.0038	0.529	0.037	0.0678	0.0018	390	150	426	25	423	11	
22	167	122	1.37	0.052	0.0042	0.482	0.041	0.0667	0.002	210	160	394	28	416	12	
23	322	214	1.50	0.0551	0.0038	0.501	0.031	0.0673	0.002	350	150	409	21	419	12	
24	230	132	1.74	0.056	0.0043	0.493	0.036	0.0651	0.002	360	160	403	24	407	12	
25	699	296	2.36	0.0543	0.0028	0.523	0.031	0.0687	0.0018	360	120	424	20	428	11	
26	548	280	1.96	0.0612	0.0042	0.554	0.035	0.0657	0.0021	570	150	445	23	410	12	
27	187	127.9	1.46	0.0572	0.0047	0.521	0.044	0.0659	0.0017	390	170	419	29	411	10	
28	209	141	1.48	0.0592	0.0047	0.548	0.039	0.0674	0.0023	480	160	439	25	421	14	
29	222	160	1.39	0.0594	0.0044	0.554	0.039	0.068	0.0022	490	160	443	25	424	13	

表 2 哈满沟变流纹岩 LA-ICP-MS 锆石微量元素组成

Table 2 LA-ICP-MS zircon trace elements and REE composition of metarhyolite from Hamangou

 10^{-6}

测点号	Sc	Ti	Y	Nb	La	Ce	Pr	Nd	Sm	Eu	Gd	Tb	Dy	Ho	Er	Tm	Yb	Lu	Hf	Ta	Th	U	Eu/Eu*	Ce/Ce*	T _{Zr} /°C		
HMG10																											
1	218	616	0.19	22.3	0.011	1.15	1.5	0.42	11.2	4.4	50.7	20.4	84.7	19.9	204	37	9240	0.17	49.5	50.3	0.31	0.93					
2	203	60	889	0.26	23.3	0.133	2.12	4.07	0.87	17.8	6.5	79.3	34.2	144	33.1	305	50.4	9050	0.5	66.7	61.6	0.31	1.07	927			
3	171	8	980		25.1		1.39	3.6	0.52	17.8	6.2	78.2	30	131	30.2	274	48.3	9690	0.53	59.4	61.9	0.20	0.93	722			
4	258	24	520	0.32	0.56	21.9	0.76	6.9	5	0.72	9.8	3.49	46.1	19	82.7	18.4	202	36.2	9410	0.46	56.1	53.9	0.31	8.23	824		
5	248	49	744		21.4	0.042	1.67	2.9	0.63	16.3	6.4	63.1	25.1	107	24.8	275	39.9	8300	0.8	53.3	54.9	0.28	0.69	903			
6	297	20	628	3.7	23.1		0.84	3.5	0.33	12.4	3.76	46.5	18.6	91	18.8	197	36.8	9300	0.29	47.3	59.5	0.15	0.73	806			
7	219	27	1890	3.1	0.27	35.9	0.51	7	12	1.84	50.5	16.2	182	72.2	283	57.9	547	100.6	8130	0.43	218	157	0.23	23.72	837		
8	247	50	663	0.67	2.6	29.9	1.02	6.3	5.5	0.98	16.8	4.84	59.4	22.5	97	23.7	231	39.2	9370	0.39	66.2	64.4	0.31	4.50	905		
9	230	19	570		18.7	0.021	0.65	1.33	0.45	9.4	3.8	45.4	20.8	94	20.3	185	38.4	8860	0.65	36.6	46	0.39		801			
10	208		1020	0.86	25.4	0.18	2.9	5.6	1.07	25.9	9.5	104	35.1	157	37.3	320	58.2	9900	0.6	87	74.1	0.27					
11	170	40	589	0.7	18.6		0.63	1.78	0.44	13.2	3.94	50.2	22	92.2	19.2	209	36.6	8770	0.44	36.7	45	0.28		879			
12	159		668	1.1	30.8	0.012	1.83	2.71	0.22	13.7	4.4	52.4	21.2	100	21.4	213	41.3	8770	0.73	58	70.6	0.11					
13	274	58	680	0.39	24.3	0.048	0.58	2.17	0.59	15.2	5.18	58.8	23.4	108	23.9	235	42.4	8420	0.33	53.2	53.5	0.314		923			
14	242	58	847		0.51	26.3	0.25	3	3.7	0.62	17.8	6.2	79	29.9	132	26.6	253	54.6	9320	0.18	68.8	69.6	0.234	18.06	923		
15	252	28	715	2.5	23.1	0.053	2.2	3.05	0.57	14.4	6.6	65.2	27	120	28	253	45.7	9260	0.59	52.6	53.9	0.263		840			
16	220	32	559		20.3	0.019	1.09	1.4	0.51	15.5	4.41	54.1	25.4	95	19.7	195	36.4	8770	0.55	41.6	45.8	0.33		855			
17	251	22	996	0.32	64	187	19	108	25.6	2.87	44.9	9.9	107	40.8	157	30.7	302	51.8	8520	0.51	73.6	61.4	0.259	1.31	815		
18	189	9	738	1.5	0.2	24.9	0.056	0.64	2.74	0.59	19.5	7.5	71.6	27.9	118	27.3	261	47.5	8650	0.24	58.9	57	0.247	57.69	732		
19	296	26	787		28	0.083	0.99	3.32	0.92	15.4	6	71.9	29.4	125	28.5	300	49.2	9710	0.61	70.8	72	0.393		833			

续表2

测点号	Sc	Ti	Y	Nb	La	Ce	Pr	Nd	Sm	Eu	Gd	Tb	Dy	Ho	Er	Tm	Yb	Lu	Hf	Ta	Th	U	Eu/Eu*	Ce/Ce*	T _{Zr} /°C	
20	238	21	967	0.34		22.8		2.1	3.5	1.04	25.4	7.9	84	37.3	164	32.6	314	61.8	9530	0.65	72.1	61	0.34		811	
21	270	1	672	2.5		22.6	0.016	1.07	2.54	0.5	16.9	5.1	64.6	24.6	103	21.3	216	41.1	9000	0.45	57.1	60.8	0.233		572	
22	178		871	2.3		39.3		1.29	2.34	0.75	14.2	5.2	65.5	33.1	148	37.5	367	75	10300	1.97	205	270	0.398			
23	415	23	2080	1.6	20.8	79	5.6	27.6	12.3	2.06	51.1	14.4	191	79.3	374	71.5	693	136	8950	1.04	474	393	0.251	1.79	820	
24	287	68	896	0.38		25.3	0.062	2.1	3.8	0.56	22.1	7.3	84.9	32.8	147	30.3	303	54.7	9290	0.56	85.9	75.1	0.19		943	
25	236	45	919			0.028	27	0.32	3.2	6.5	0.71	25.6	8.1	103	36.4	157	34.8	285	57.9	8150	0.56	93.5	70.4	0.168	69.93	893
26	158	14	922			21.9		0.85	5.4	0.97	22.9	6.83	103	35.1	148	30.7	322	54.4	8870	0.64	74.5	63.5	0.267		771	
27	239	38	569	0.8	0.39	22.9	0.075	1.76	2.61	0.43	12	4.01	59.6	23.5	111	21.9	210	41.3	8390	0.54	56.9	57.6	0.235	32.83	874	
28	271		990	1.5		28.5	0.1	3	5.4	1.07	27	9.3	103	41.9	149	29.6	329	58.7	9370	0.58	79	79.2	0.27			
29	206	25	620			21.4		1.85	2.71	0.69	17.7	5.5	65	24.5	125	28.5	243	46.9	8190	0.33	63	64.2	0.305		828	
30	219		611			0.096	20.3		0.9	2.11	0.4	13.9	4.32	60.8	24.5	99	19.5	198	38.1	8540	0.4	45.7	49.5	0.226	18.43	
HMG12																										
1	236	12	1650	3.6		78.6	0.24	3.8	6.8	2.7	44.5	13.7	150	64	277	55	504	95.8	7500	0.76	297	183	0.47	0.93	757	
2	274	2	1920	0.33		41.9	0.29	6.3	11.1	3.23	47.9	16.7	179	65	304	63.3	560	96.6	7230	0.7	163	120	0.43	1.07	617	
3	330	24	2130	2.7	440	920	120	600	118	17	137	22.9	207	68	287	57	560	103	8000	0.8	197	142	0.41	0.98	824	
4	324	49	1440	3.5	0.03	53.5	0.3	3.2	7.7	2.59	39.4	10.6	130	47.8	224	43.6	428	80	8930	0.67	111	94.5	0.45	138.27	903	
5	280	13	1620	0.7	0.2	60	0.18	3.6	6.2	2.32	31.1	11	136	53.8	273	47.9	499	100	8370	1.25	158	135	0.51	77.53	765	
6	316		2390	3.2	6.6	95	1.73	7.1	10.7	3.83	56	19.3	193	83	378	71	730	131	7350	1.36	318	209	0.48	6.89		
7	254	12	995			0.69	31.6	0.57	4.2	5.2	2.09	25.5	7	83.6	35	165	31.2	292	56.7	7050	0.48	127	87	0.55	12.35	757
8	238	25	1610	2.3		77.6	0.17	2.8	6.5	2.08	39.2	11.7	134	53.1	248	45.6	464	81.3	7370	1.19	297	200	0.40	4.50	828	
9	286	42	2070	7.1		86.6	0.18	5.3	7.1	2.73	49.7	15.2	194	71.6	319	65.4	548	114.3	7490	1.01	465	256	0.44		885	
10	174	2	2070	1.9	0.036	69.9	0.18	3.8	10	3.32	52.8	14.4	192	70.5	327	62.9	597	108	8080	1.43	223	166	0.44	212.90	617	
11	323	17	2690	0.36	0.034	36.4	0.55	9.1	15.8	9.7	93	25.4	254	89.6	428	86	727	145	6770	0.42	213	116	0.77	65.26	790	
12	274	10	1260	0.39		35.1	0.106	1.81	6.3	2.02	24.1	9.2	101	43.7	220	42.7	429	79.8	7510	0.64	89	86.3	0.50		741	
13	261	3	3330	0.34	52	198	16.2	75	28.5	6.47	96	28.7	302	107	476	102	896	155	8860	0.91	324	221	0.378	1.67	645	
14	221	19	1570	1.1	0.42	77.1	0.24	4	7.7	2.45	41.5	13.1	145	53.3	233	50.5	430	86.8	6940	1.32	381	198	0.419	59.54	801	
15	267		2450	2.2	0.017	76.3	0.42	4.2	11.9	4.14	63.8	21.8	227	89	372	74.7	663	121	8440	1.13	245	189	0.459	221.39		
16	254	21	3030	0.33		57.4	0.36	10.2	16.2	6.38	82	25.6	248	97.3	444	85	877	157	7690	0.68	289	180	0.54		811	
17	298	45	2090			51.8	0.35	2.5	9	3.92	48.4	11.5	171	64.2	298	61.1	554	104.6	6660	0.55	214	126.4	0.574	1.31	893	
18	356	22	2830	2.6	0.014	65.6	0.48	5.6	15.6	6.11	80	24.3	240	94.3	422	92	850	154	6230	0.83	312	183	0.529	196.20	815	
19	293	7	4360	1.5		101	0.49	13.4	22.5	11.9	140	40.4	394	142	644	118	1050	193	7480	0.81	683	250	0.648		711	
20	293	20	2430	1.9	42.6	193	12.8	64	23.8	5.58	71	21.4	211	83	369	78	675	118	8600	1.05	404	245	0.41	2.03	806	
21	323		2920	0.9	0.062	55.5	0.64	8.3	15.7	6.33	79	21.8	264	93	461	88	793	144	7050	0.75	239	160	0.549	68.31		
22	251	48	2370	0.8	0.022	45.3	0.19	6.2	12.8	5.62	63	19	214	84.1	364	69.5	720	121	7670	0.29	167	122	0.605	171.79	901	
23	276	18	1910	2.4	0.053	81.8	0.016	3.9	7.2	2.6	42.6	13.2	160	65.6	293	60.8	570	105	8120	1.17	322	214	0.454	688.72	795	
24	244	15	3070			0.017	70.8	0.6	12.5	24.3	8.55	106	29.7	320	106	495	94	840	139	6930	1.02	230	132	0.52	171.88	778
25	271	2	3440	0.8	39	231	12.6	60	30	8.2	95	30	317	112	463	95	860	142	7200	1.38	699	296	0.47	2.55	617	
26	292		2720	2.3	19.6	150	6.9	36.8	19.6	5.73	83.1	20.8	281	93	385	78.2	790	140	7620	0.96	548	280	0.434	3.16		
27	263	25	2180	0.34		44.3	0.51	7.1	12.6	5.49	57.9	18.9	206	72.3	351	64.4	650	114.2	7290	0.44	187	127.9	0.621	32.83	828	
28	265	76	1570	2.1	0.087	53.4	0.11	2.4	6.3	2.56	38.6	10.8	151	52.5	229	48.5	496	88	7500	0.83	209	141	0.50	133.84	957	
29	360	3	1780	0.48	18	96	5.8	31.5	11.9	3.29	41.3	12.8	152	57.5	271	57.4	572	108	7200	0.93	222	160	0.454	2.30	645	

注:空白表示低于检测线

带且没有裂缝或包裹体发育的锆石边部。结果显示,29个测试点的年龄数据均落在U-Pb年龄谐和

线上且年龄值相对集中,主要介于436~407 Ma之间,年龄加权平均值为417.7±4.4 Ma(MSWD=0.30)

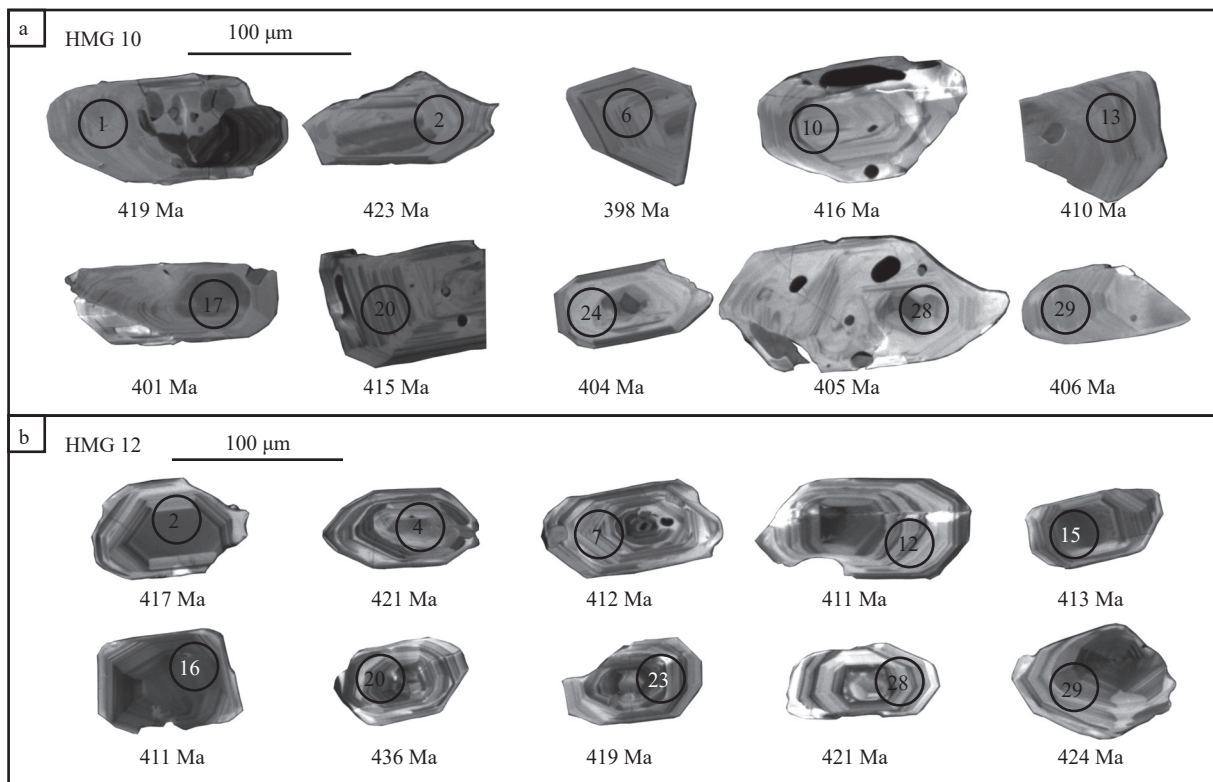


图4 南天山造山带哈满沟地区变流纹岩代表性锆石阴极发光(CL)图像及其测点的位置与编号

Fig. 4 CL images of the representative zircons from the metarhyolites of the Hamangou area in the South Tianshan Orogenic Belt and their corresponding locations and numbers of analytical points

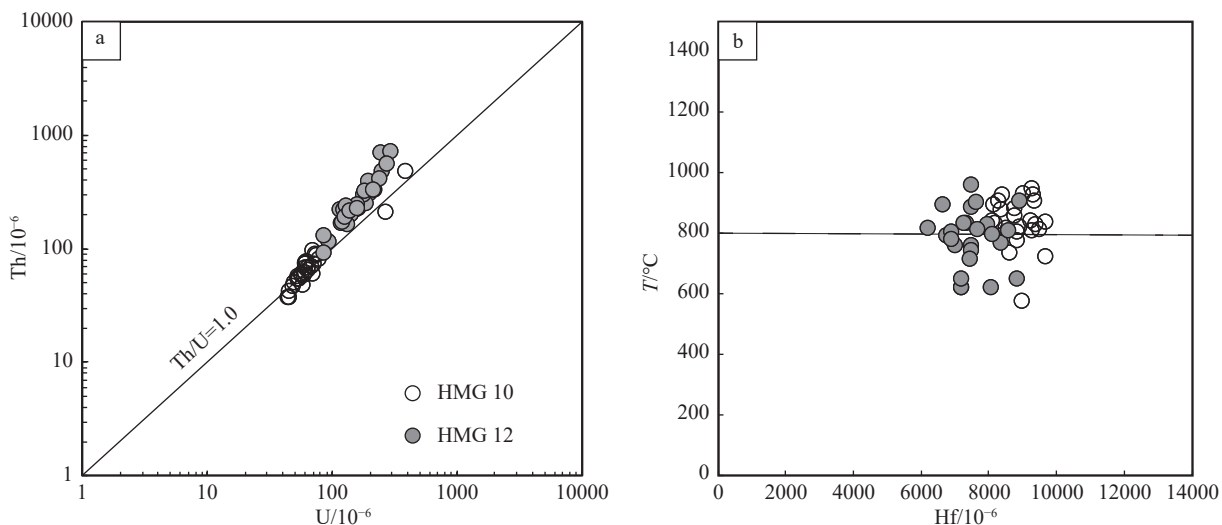


图5 南天山造山带哈满沟地区变流纹岩锆石U-Th图解(a)和锆石结晶温度与Hf含量关系图(b)

Fig. 5 U-Th diagram (a) and relationship between crystallization temperature and Hf content (b) of zircon from metarhyolites of the Hamangou area in the South Tianshan Orogenic Belt

(图6-c,d),代表了变流纹岩原岩的岩浆喷发时代。

3.2 锆石微量元素特征

本次分别测定了HMG10和HMG12两件变流纹岩样品锆石的微量和稀土元素含量,并据此绘制

球粒陨石标准化稀土元素配分曲线图(图7-a,c)和微量元素蛛网图(图7-b,d)。

HMG10样品锆石的稀土元素总量(Σ REE)为 $438.25 \times 10^{-6} \sim 1757.66 \times 10^{-6}$,轻稀土元素(LREE)含量

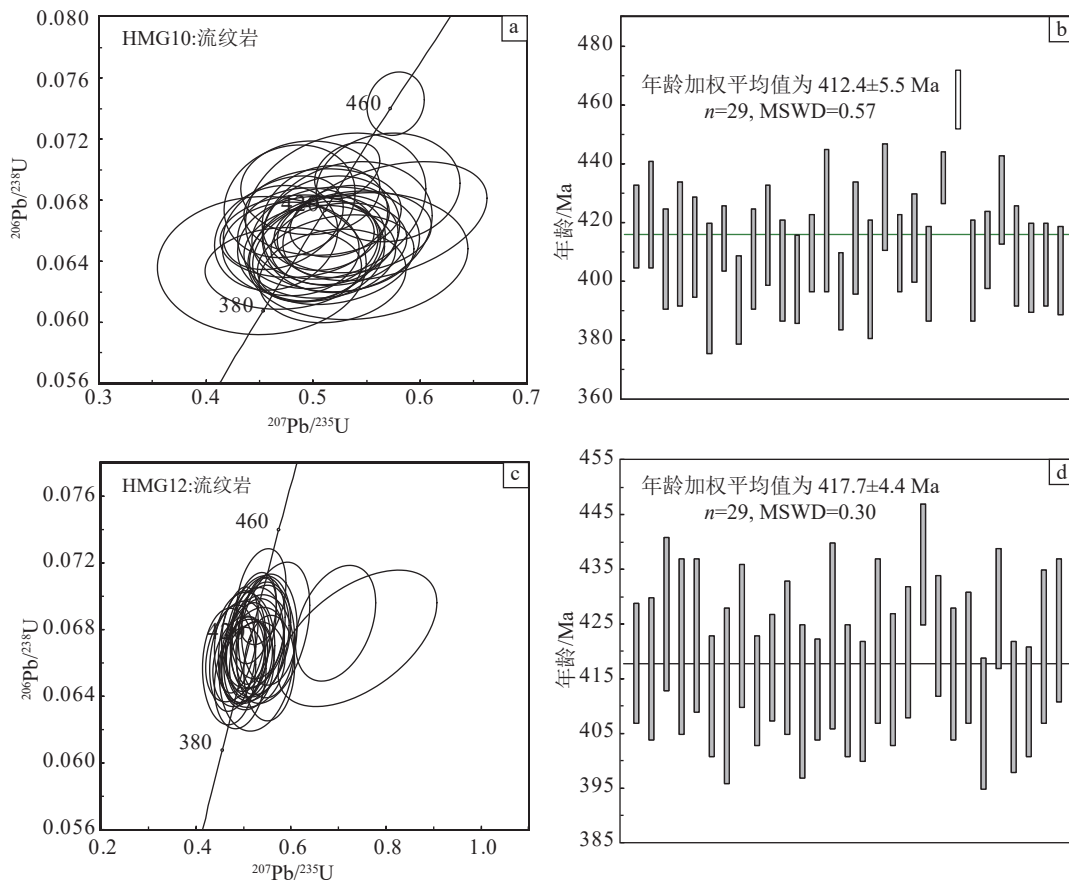


图 6 南天山造山带哈满沟地区变流纹岩的锆石年龄谐和图(a, c)和 $^{206}\text{Pb}/^{238}\text{U}$ 年龄分布直方图及其年龄加权平均值(b, d)

Fig. 6 Zircon U-Pb concordia diagrams (a, c) and $^{206}\text{Pb}/^{238}\text{U}$ age histograms and their weighted mean ages (b, d) of the metarhyolites from the Hamangou area in the South Tianshan Orogenic Belt

为 $21.15 \times 10^{-6} \sim 406.47 \times 10^{-6}$, 重稀土元素(HREE)含量为 $417.10 \times 10^{-6} \sim 1610.30 \times 10^{-6}$ 。球粒陨石标准化稀土元素配分曲线显示, 轻稀土元素相对亏损, 重稀土元素相对富集。 Eu/Eu^* 值为 $0.11 \sim 0.40$, Ce/Ce^* 值为 $0.69 \sim 69.93$, 显示负 Eu 异常、正 Ce 异常的特征(图 7-a), 进一步表明这些锆石是岩浆成因的锆石(吴元保和郑永飞, 2004; 雷玮琰等, 2013)。锆石中 Hf 含量较高($8130 \times 10^{-6} \sim 10300 \times 10^{-6}$)。此外, 还有效测定了高场强元素 Nb、Ta 和 Ti 元素的含量, 锆石 Nb 含量($0.19 \times 10^{-6} \sim 3.7 \times 10^{-6}$)、Ta 含量($0.17 \times 10^{-6} \sim 1.97 \times 10^{-6}$)、Ti 含量($1 \times 10^{-6} \sim 68 \times 10^{-6}$)均在岩浆锆石范围内(Hoskin et al., 2003)。

HMG12 样品的锆石稀土元素总含量($740.35 \times 10^{-6} \sim 3656.90 \times 10^{-6}$)高于 HMG10 样品, 轻稀土元素含量为 $44.35 \times 10^{-6} \sim 2215.00 \times 10^{-6}$, 重稀土元素含量为 $696.00 \times 10^{-6} \sim 2721.40 \times 10^{-6}$, 在球粒陨石标准化的稀土元素配分曲线上也具有轻稀土元素相对亏损、

重稀土元素相对富集的特点。 Eu/Eu^* 值($0.38 \sim 0.77$)、 Ce/Ce^* 值($0.93 \sim 688.72$)同样显示负 Eu 异常、正 Ce 异常的特征(图 7-a), 表明这些锆石是岩浆成因(吴元保和郑永飞, 2004; 雷玮琰等, 2013)。此外, 还测定了锆石中的 Hf 含量($6230 \times 10^{-6} \sim 8930 \times 10^{-6}$)、Nb 含量($0.33 \times 10^{-6} \sim 7.1 \times 10^{-6}$)、Ta 含量($0.29 \times 10^{-6} \sim 1.43 \times 10^{-6}$)和 Ti 含量($2 \times 10^{-6} \sim 76 \times 10^{-6}$), 也均落在岩浆锆石特征范围内(Hoskin et al., 2003)。

4 讨 论

4.1 变流纹岩原岩形成时代

本次研究的变流纹岩样品采集自兴地塔格群辛格尔组(中亚组)。前人认为辛格尔组属于太古宙地层, 主要发育大理岩, 有时相变为灰色绢云母石英片岩和黑云母片岩(新疆维吾尔自治区地质矿产局, 1993)。中亚组发育灰绿色黑云角闪石英斜长片岩, 局部为大理岩。然而, 辛格尔组(中亚组)的时代一

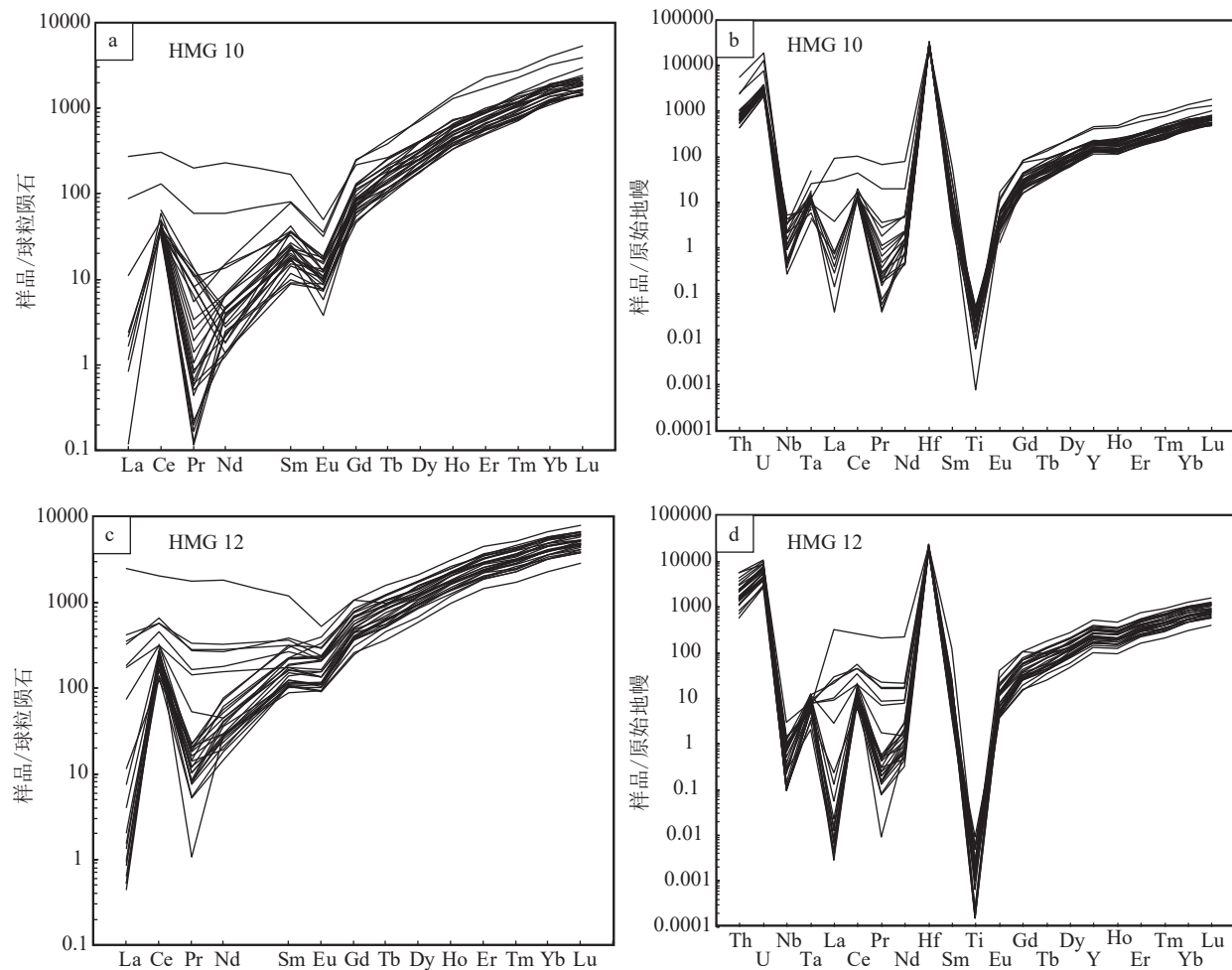


图 7 南天山造山带哈满沟地区变流纹岩锆石球粒陨石标准化稀土元素配分曲线图(a, c)和微量元素蛛网图(b, d)

(标准化值据 McDonough et al., 1995)

Fig. 7 Chondrite-normalized REE contents diagrams (a, c) and multi-elements spider diagrams (b, d) of zircons from the metarhyolites of the Hamangou area in the South Tianshan Orogenic Belt

直没有很好地限定。本次定年结果表明,变流纹岩主要形成于 418~412 Ma,是南天山造山带南缘早泥盆世火山喷发的产物。此外,野外地质调查显示,辛格尔组内也发育片岩,定年结果指示其原岩沉积时代也为泥盆纪(待发表)。因此,根据本次测年结果,库尔勒北部辛格尔组变流纹岩及其相邻层段片岩原岩的形成时代应不是太古宙,而是早泥盆世。

4.2 锆石微量元素及地质意义

锆石的物理化学性质相对稳定,U-Th-Pb 同位素体系具有较高的封闭温度,在地质演化过程中除 U、Th 等元素衰变外,锆石中其他元素可以保持其初始的化学组分(Hoskin et al., 2003; El-Bialy et al., 2013; 周敖日格勒等,2017)。锆石结晶过程中趋于吸收 Sc、Y、Ti、Hf、Th、U、Nb、Ta、V、P 和 REE 等

特定的微量元素,这些元素的含量对锆石形成的地质过程具有一定的指示作用(El-Bialy et al., 2013; 周敖日格勒等,2017)。前人对锆石微量元素开展了大量研究并取得丰硕成果,如利用 U-Th-Pb 同位素获得结晶年龄(Schoene, 2014),利用锆石 Ti 温度计估算锆石结晶温度(Watson et al., 2005),利用锆石 Eu 异常计算地壳厚度(Tang et al., 2020)和氧逸度(Smythe et al., 2015, 2016; Loucks et al., 2020),区分锆石源区(Grimes et al., 2015),并记录岩浆源区(吴福元等, 2005; Kemp et al., 2006; Dai et al., 2011)、岩浆演化过程(Yan et al., 2018, 2020)、构造背景(Yang et al., 2012; Carley et al., 2014)等信息。

4.2.1 锆石微量元素对岩浆作用过程的指示

锆石微量元素的含量变化可以反映其形成的地

质环境。如 U/Yb 值可用来指示不同源区来源的锆石,其中大洋辉长岩的 U/Yb 值在 0.18 左右,陆壳花岗岩的 U/Yb 值在 1.07 左右,而金伯利岩的 U/Yb 值在 2.1 左右(Grimes et al., 2007; 周敖日格勒等, 2017)。基于此,有研究者使用 $Y-U/Yb$ 和 $Hf-U/Yb$ 判别图解来区分锆石来源(Grimes et al., 2007)。在 $Y-U/Yb$ 和 $Hf-U/Yb$ 判别图解中,研究区 2 件流纹岩样品的锆石数据点均投在陆壳区域(图 8),指示变流纹岩锆石主要形成于陆壳环境,推断南天山造山带南缘泥盆纪中酸性侵入岩体结晶环境为陆壳环境。锆石的 Ce、Eu 异常主要受控于结晶时的物理化学条件。有研究表明,岩浆来源小于 35 km 时会有明显的负 Eu 异常,而大于 35 km 则有弱的负 Eu 异常或无负 Eu 异常(Barth et al., 2010; Claiborne et al., 2010; Trail et al., 2012; Burnham et al., 2012; Li et al., 2012; 周敖日格勒等, 2017)。本次研究的 HMG10 变流纹岩的 Eu/Eu^* 值介于 0.11~0.40 之间, Ce/Ce^* 值介于 0.69~69.93 之间,HMG12 变流纹岩的 Eu/Eu^* 值介于 0.38~0.77 之间, Ce/Ce^* 值介于 0.93~688.72 之间,均表现出强的负 Eu 异常和正 Ce 异常,表明泥盆纪流纹岩的岩浆源区深度小于 35 km,指示流纹岩喷发时期不存在明显的地壳增厚作用。

此外,锆石中的 Ce 和 Eu 元素不同于其他稀土元素,Ce 和 Eu 离子有 2 种价态,Ce 异常和 Eu 异常的变化可以反映锆石结晶的物理化学条件(Trail et al., 2012; 黄永高等, 2019)。在氧化条件下, Ce^{3+} 一旦

氧化成 Ce^{4+} ,Ce 元素比其他 LREE 元素更容易进入锆石晶体,导致在岩浆锆石球粒陨石标准化稀土元素配分曲线上显示 Ce 比 La 和 Pr 更富集的特征;在还原条件下, Eu^{3+} 还原成 Eu^{2+} ,更难进入锆石晶体,在岩浆锆石球粒陨石标准化稀土元素配分曲线上显示 Eu 比 Sm 和 Gd 更亏损的特征(Trail et al., 2012; 周敖日格勒等, 2017; 黄永高等, 2019)。本次研究样品的 Ce 比 La 和 Pr 更富集,Eu 比 Sm 和 Gd 更亏损,反映氧化条件和还原条件同时存在。然而,氧化环境和还原环境在锆石中同时出现是相互对立的,即氧逸度不能同时控制负 Eu 异常及正 Ce 异常(El-Bialy et al., 2013; 周敖日格勒等, 2017; 黄永高等, 2019),说明锆石中 Eu、Ce 异常还受其他因素控制。研究表明,另一个导致岩浆锆石负 Eu 异常的重要因素是,在锆石结晶前或结晶过程中岩浆源区存在斜长石的分离结晶作用(Hoskin et al., 2000, 2003; Kaczmarek et al., 2008; Burnham et al., 2012)。因此,笔者认为,本次研究的泥盆纪变流纹岩在成岩过程中可能存在斜长石的分离结晶作用。

4.2.2 锆石微量元素对流纹岩形成构造背景的约束

岩浆的形成和演化受构造背景控制,不同构造背景下形成的岩浆成分和性质不同,从而导致岩浆冷却结晶时锆石中赋存的微量元素特征也具有显著的差异(王森等, 2019)。有学者提出,利用锆石微量元素可以很好地判别该时期岩浆作用的构造背景(Schulz et al., 2006; Yang et al., 2012; Carley et al.,

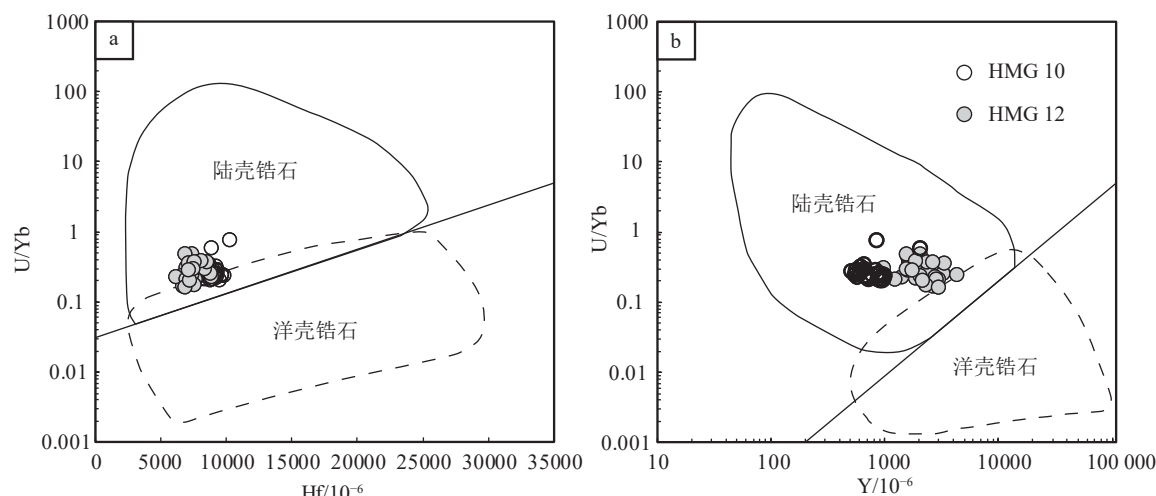


图 8 南天山哈满沟地区变流纹岩锆石来源判别图(据 Grimes et al., 2007 修改)

Fig. 8 Source discrimination diagrams of the zircons of the meta rhyolite in the Hamangou region of the South Tianshan (after Yang et al., 2012)

2014)。Yang et al.(2012)利用锆石微量元素建立了Th/U-Nb/Hf和Th/Nb-Hf/Th构造背景判别图,用来判别锆石的形成背景。本次研究的变流纹岩样品(HMG10和HMG12)在Th/U-Nb/Hf和Th/Nb-Hf/Th图解中都处于汇聚岛弧/造山构造环境(图9),表明南天山造山带南缘在泥盆纪可能存在与汇聚岛弧或造山相似的岩浆活动背景。Lin et al. (2013)对南天山造山带南缘泥盆纪侵入岩进行了岩石地球化学研究,结果显示,这些侵入岩富集轻稀土元素,相对亏损重稀土元素,具弱负Eu异常,富集大离子亲石元素Ba、K,亏损高场强元素Nb、Ta。此外,富集Pb、亏损Ti,显示典型的岛弧岩浆岩地球化学特征。它们与塔里木克拉通北缘早古生代俯冲背景形成的岩浆岩相似(Ge et al., 2012)。以上研究表明,塔里木克拉通北缘和南天山造山带在早古生代存在岩浆弧,指示这一时期南天山造山带北缘发育向南的洋-陆俯冲体系。

值得注意的是,本次使用锆石Ti温度计($\log(T_{\text{Zircon}})=6.01\pm0.03-(5080\pm30)/(T(\text{K}))$)估算了变流纹岩锆石的结晶温度。结果表明,变流纹岩锆石普遍显示出较高的结晶温度。HMG10变流纹岩的原岩岩浆结晶温度为527~943℃,平均835℃,HMG12变流纹岩样品的原岩岩浆结晶温度为619~957℃,平均779℃,大部分大于800℃(图5-b),指示变流纹岩的成岩温度较高。研究表明,A型花

岗岩或由地幔柱作用形成的花岗岩结晶温度较高,其结晶温度一般大于800℃(吴福元等,2007;周敖日格勒等,2017;黄永高等,2019;李壮等,2022)。变流纹岩成岩温度较高,具有A型花岗岩的特征,而A型花岗质岩浆的出现往往与地幔柱或软流圈物质上涌、区域构造伸展密切关联。同时,在Y-Lu/Hf(图10-a)图解中,流纹岩样品主要位于火山弧和板内区域,在Y-Yb/Dy图解(图10-b)中,流纹岩样品也接近火山弧和板内区域,指示其可能形成于陆缘弧后裂谷环境(图10)。前人研究(王博等,2013;Wang et al., 2018b)认为,早古生代塔里木克拉通北缘为活动陆缘环境,早古生代早期南天山洋向南俯冲,即俯冲于中天山-塔里木克拉通北缘之下,发育岛弧岩浆岩;晚志留世—早泥盆世,塔里木克拉通岛弧岩浆作用减弱,弧后伸展形成南天山弧后洋盆,将中天山地块从塔里木克拉通北缘分离出来;晚古生代,南天山洋持续俯冲消减,南天山弧后盆地可能也随之关闭,最终形成复杂的南天山造山带。此外,南天山造山带内部还识别出多条蛇绿岩带,根据其产出位置大致分为北带和南带。其中,北带蛇绿岩显示为MORB型特征,即含有典型的洋脊玄武岩(MORB)和洋岛玄武岩(OIB),可能代表了南天山洋盆俯冲消减和闭合过程。南带蛇绿岩具有SSZ型特征,即形成于俯冲带上(supra-subduction zone),可能是南天山弧后洋盆消减关闭的产物(王博等,2022)。综上

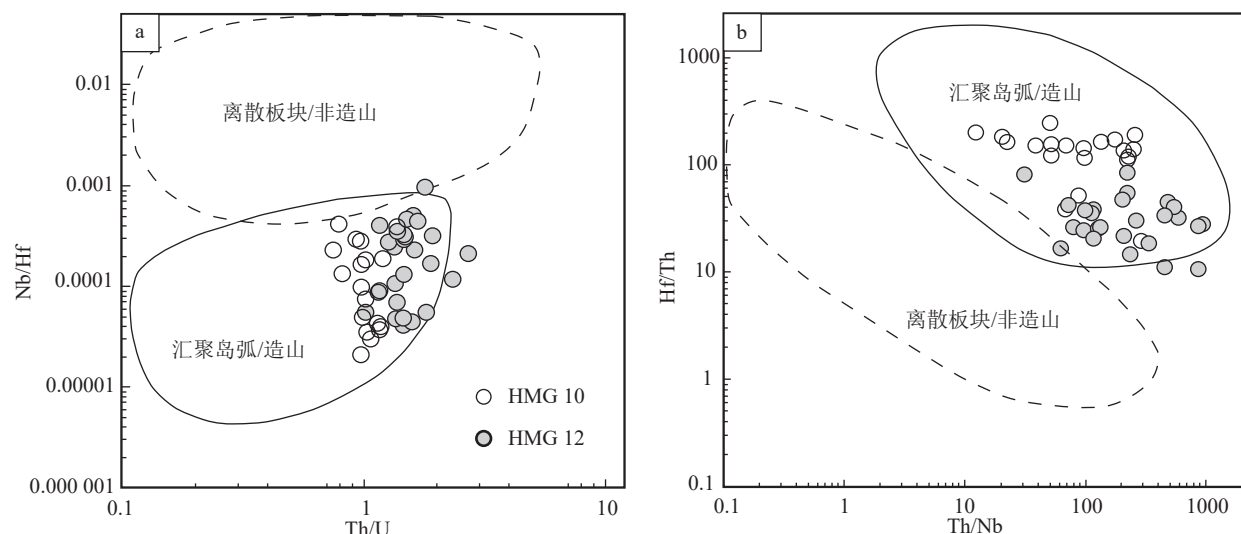


图9 南天山哈满沟地区变流纹岩锆石微量元素构造背景判别图(据 Yang et al., 2012)

Fig. 9 Tectonic background discrimination diagrams of zircon trace elements of the meta rhyolite in the Hamangou region of the South Tianshan

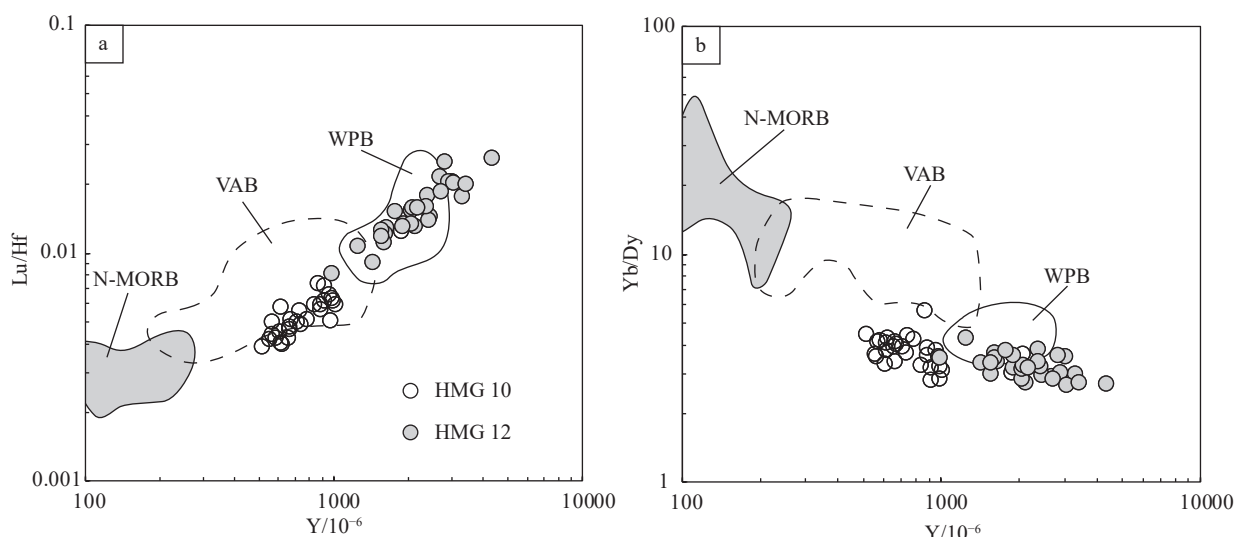


图 10 不同构造背景下锆石的判别图解(据 Schulz et al., 2006)

Fig. 10 Discrimination plots of different tectonic settings for the zircon
N-MORB—正常洋中脊玄武岩; VAB—火山弧玄武岩; WPB—板内玄武岩

分析提出,本次研究的变流纹岩原岩是陆缘裂谷盆地发育阶段火山喷发的产物,其形成可能与南天山洋早泥盆世俯冲后撤、弧后伸展有关。

5 结 论

(1) 南天山造山带东段哈满沟地区变流纹岩原岩主要形成于早泥盆世(418~412 Ma)。

(2) 早泥盆世流纹岩是高温岩浆喷发作用的产物,具有与 A 型花岗岩相似的地球化学特征,其岩浆源区深度小于 35 km, 岩浆结晶过程中可能存在斜长石分离结晶。

(3) 南天山造山带哈满沟地区早泥盆世流纹岩形成于陆缘裂谷背景,可能与晚志留世—泥盆纪南天山洋俯冲后撤、弧后伸展等构造过程有关。

致谢:浙江大学地球科学学院陈汉林教授、吴鸿翔博士后,仇度伟、尹启航、雷钰薇、田禾丰博士生等在野外地质调查和样品采集过程中提供了帮助;两位审稿专家细致审阅初稿,并提出了建设性修改意见和建议,对论文质量提升有很大帮助,在此一并表示衷心的感谢。

References

- Bai J K, Li Z P, Xu X Y, et al. 2015. Tectonic Environment of Western Tianshan during the Early Carboniferous: Sedimentary and stratigraphical evidence from the bottom of the Dahalajunshan Formation[J]. *Acta Sedimentological Sinica*, 33(3): 459–469 (in Chinese with English abstract).

abstract).

Barth A P, Wooden J L. 2010. Coupled elemental and isotopic analyses of polygenetic zircons from granitic rocks by ion microprobe, with implications for melt evolution and the sources of granitic magmas[J]. *Chemical Geology*, 277(1/2): 149–159.

Burnham A D, Berry A J. 2012. An experimental study of trace element partitioning between zircon and melt as a function of oxygen fugacity[J]. *Geochimica et Cosmochimica Acta*, 95: 196–212.

Carley T L, Miller C F, Wooden J L, et al. 2014. Iceland is not a magmatic analog for the Hadean: Evidence from the zircon record[J]. *Earth and Planetary Science Letters*, 405: 85–97.

Claiborne L L, Miller C F, Wooden J L. 2010. Trace element composition of igneous zircon: A thermal and compositional record of the accumulation and evolution of a large silicic batholith, Spirit Mountain, Nevada[J]. *Contributions to Mineralogy and Petrology*, 160(4): 511–531.

Dai L Q, Zhao Z F, Zheng Y F, et al. 2011. Zircon Hf–O isotope evidence for crust–mantle interaction during continental deep subduction[J]. *Earth and Planetary Science Letters*, 308(1/2): 229–244.

El-Bialy M Z, Ali K A. 2013. Zircon trace element geochemical constraints on the evolution of the Ediacaran (600–614 Ma) post-collisional Dokhan volcanics and Younger granites of SE Sinai, NE Arabian–Nubian Shield[J]. *Chemical Geology*, 360–361: 54–73.

Gao J, Qian Q, Long L, I, et al. 2009. Accretionary orogenic process of Western Tianshan, China[J]. *Geological Bulletin of China*, 28(12): 1804–1816 (in Chinese with English abstract).

Ge R F, Zhu W B, Wu H L, et al. 2012. The Paleozoic northern margin of the Tarim Craton: Passive or active? [J]. *Lithos*, 142/143: 1–15.

Grimes C B, John B E, Kelemen P B, et al. 2007. Trace element chemistry of zircons from oceanic crust: A method for distinguishing detrital zircon provenance[J]. *Geology*, 35(7): 643–646.

- Grimes C B, Wooden J L, Cheadle M J, et al. 2015. "Fingerprinting" tectono-magmatic provenance using trace elements in igneous zircon[J]. *Contributions to Mineralogy and Petrology*, 170(5): 46.
- Guo R Q, Qin Q, Muhetaer Z R, et al. 2013. Geological characteristics and tectonic significance of Ordovician granite intrusions in the western segment of Quruqtagh, Xinjiang[J]. *Earth Science Frontiers*, 20(4): 251–263 (in Chinese with English abstract).
- Han Y G, Zhao G C, Sun M, et al. 2015. Paleozoic accretionary orogenesis in the Paleo-Asian Ocean: insights from detrital zircons from Silurian to Carboniferous strata at the north-western margin of the Tarim Craton[J]. *Tectonics*, 34: 334–351.
- Han Y G, Zhao G C, Sun M, et al. 2016. Late Paleozoic subduction and collision processes during the amalgamation of the Central Asian orogenic belt along the South Tianshan suture zone[J]. *Lithos*, 246: 1–12.
- Han Y G, Zhao G C. 2018. Final amalgamation of the Tianshan and Junggar orogenic collage in the southwestern Central Asian Orogenic Belt: Constraints on the closure of the Paleo-Asian Ocean[J]. *Earth-Science Reviews*, 186: 129–152.
- Hoskin P W O, Ireland T R. 2000. Rare earth element chemistry of zircon and its use as a provenance indicator[J]. *Geology*, 28(7): 627–630.
- Hoskin P W O, Schaltegger U. 2003. The composition of zircon and igneous and metamorphic petrogenesis[J]. *Reviews in Mineralogy and Geochemistry*, 53(1): 27–62.
- Huang H, Wang T, Tong Y, et al. 2020. Rejuvenation of ancient micro-continents during accretionary orogenesis: insights from the Yili block and adjacent regions of the SW Central Asian Orogenic Belt[J]. *Earth-Science Reviews*, 208: 103255.
- Huang H, Zhang Z C, Santosh M, et al. 2018. Crustal evolution in the South Tianshan Terrane: Constraints from detrital zircon geochronology and implications for continental growth in the Central Asian orogenic belt[J]. *Geological Journal*, 54(3): 1379–1400.
- Huang Y G, Luo G, Zhang T, et al. 2019. LA-CP-MS zircon U-Pb dating and trace element geochemistry of Xiaoqiaotou porphyry in Lijiang, western Yunnan[J]. *Journal of Guilin University of Technology*, 39(1): 26–37 (in Chinese with English abstract).
- Jahn, B M. 2004. The Central Asian Orogenic Belt and growth of the continental crust in the Phanerozoic[J]. *Geological Society, London: Special Publications*, 226(1): 73–100.
- Jiang T, Gao J, Klemd R, et al. 2014. Paleozoic ophiolitic mélange from the South Tianshan Orogen, NW China: Geological, geochemical and geochronological implications for the geodynamic setting[J]. *Tectonophysics*, 612: 106–127.
- Jiang T, Gao J, Klemd R, et al. 2015. Genetically and geochronologically contrasting plagiogranites in South Central Tianshan ophiolitic mélange: Implications for the breakup of Rodinia and subduction zone processes[J]. *Journal of Asian Earth Sciences*, 113: 266–281.
- Kaczmarek M A, Müntener O, Rubatto D. 2008. Trace element chemistry and U-Pb dating of zircons from oceanic gabbros and their relationship with whole rock composition (Lanzo, Italian Alps)[J]. *Contributions to Mineralogy and Petrology*, 155(3): 295–312.
- Kemp A I S, Hawkesworth C J, Paterson B A, et al. 2006. Episodic growth of the Gondwana supercontinent from hafnium and oxygen isotopes in zircon[J]. *Nature*, 439(7076): 580–583.
- Klemd R, Gao J. 2015. Metamorphic evolution of(ultra)-high-pressure subduct ion-related transient crust in the South Tianshan Orogen (Central Asian orogenic belt): geodynamic implications[J]. *Gondwana Research*, 28(1): 1–25.
- Klemd R, John T, Scherer E, et al. 2011. Changes in dip of subducted slabs at depth: Petrological and geochronological evidence from HP-UHP rocks (Tianshan, NW-China)[J]. *Earth and Planetary Science Letters*, 310(1/2): 9–20.
- Konopelko D, Biske G, Setmann R, et al. 2007. Hercynian post-collisional A-type granites of the Kokshaal Range, Southern Tien Shan, Kyrgyzstan[J]. *Lithos*, 97(1/2): 140–160.
- Konopelko D, Seltmann R, Biske G, et al. 2009. Possible source dichotomy of contemporaneous post-collisional barren I-type versus tin-bearing A-type granites, lying on opposite sides of the South Tien Shan suture[J]. *Ore Geology Reviews*, 35(2): 206–216.
- Lei W Y, Shi G H, Liu Y X. 2013. Research progress on trace element characteristics of zircons of different origins[J]. *Earth Science Frontiers*, 20(4): 273–284 (in Chinese with English abstract).
- Li N, Chen Y J, Pirajno F, et al. 2012. LA-ICP-MS zircon U-Pb dating, trace element and Hf isotope geochemistry of the Heyu granite batholith, eastern Qinling, central China: Implications for Mesozoic tectono-magmatic evolution[J]. *Lithos*, 142/143: 34–47.
- Li T Y, Jin C, Tian Z H, et al. 2022. Hf Isotopic and geochronological characteristics of Mesozoic granites and xenoliths in Rushan area and its implication on crustal evolution of Jiaodong Peninsula[J]. *Earth Science*, 47(8): 2951–2967 (in Chinese with English abstract).
- Li Y J, Yang H J, Zhao Y, et al. 2009. Tectonic framework and evolution of South Tianshan, NW China[J]. *Geotectonica et Metallogenica*, 33(1): 94–104 (in Chinese with English abstract).
- Li Z, Li X Y, Zhang P, et al. 2022. Zircon trace elemental characteristics and its geological significance of the Miocene intermediate-acid magmatic rocks in the Pusangguo deposit in Xizang[J]. *Geological Review*, 68(4): 1236–1260 (in Chinese with English abstract).
- Lin W, Chu Y, Ji W B, et al. 2013. Geochronological and geochemical constraints for a middle Paleozoic continental arc on the northern margin of the Tarim block: Implications for the Paleozoic tectonic evolution of the South Chinese Tianshan[J]. *Lithosphere*, 5(4): 355–381.
- Liu G P, Guo R Q, Cai H M, et al. 2020. U-Pb geochronology of detrital zircon in sediments from Kizil River South Tianshan, Xinjiang and its geological significance[J]. *Chinese Journal of Geology*, 56(1): 210–236 (in Chinese with English abstract).
- Liu G P. 2021. Paleozoic crustal growth and evolution in the South Tianshan Orogenic Belt—Constraints from geochronology and Hf isotopic composition of detrital zircons from the modern river[D]. PhD Dissertation of China University of Mining and Technology (in Chinese with English abstract).
- Loucks R R, Fiorentini M L, Hendquez G J. 2020. New magmatic

- oxybamometer using trace elements in zircon[J]. *Journal of Petrology*, 61(3): gaa034.
- McDonough W F, Sun S S. 1995. The composition of the earth[J]. *Chemical Geology*, 120(3/4): 223–253.
- Ning J, Jiang Y D, Schulmann K, et al. 2023. Silurian–Devonian lithospheric thinning and thermally softening along the northern margin of the Tarim Craton: Geological mapping, petro–structural analysis and geochronological constraints[J]. *Tectonics*, e2023TC007792.
- Paton C, Woodhead J D, Hellstrom J C, et al. 2010. Improved laser ablation U–Pb zircon geochronology through robust downhole fractionation correction[J]. *Geochemistry Geophysics Geosystems*, 11: Q0AA06.
- Schoene B. 2014. U–Th–Pb geochronology—ScienceDirect[C]//Treatise on Geochemistry (Second Edition). New York: Elsevier, 4: 341–378.
- Schulz B, Klemd R, Brätz H. 2006. Host rock compositional controls on zircon trace element signatures in metabasites from the Austroalpine basement[J]. *Geochimica et Cosmochimica Acta*, 70(3): 697–710.
- Smythe D J, Brenan J M. 2015. Cerium oxidation state in silicate melts: Combined f_{O_2} , temperature and compositional effects[J]. *Geochimica et Cosmochimica Acta*, 170: 173–187.
- Smythe D J, Brenan J M. 2016. Magmatic oxygen fugacity estimated using zircon–melt partitioning of cerium[J]. *Earth and Planetary Science Letters*, 453: 260–266.
- Tang M, Ji W Q, Chu X, et al. 2020. Reconstructing crustal thickness evolution from europium anomalies in detrital zircons[J]. *Geology*, 49(1): 76–80.
- Trail D, Watson E B, Tailby N D. 2012. Ce and Eu anomalies in zircon as proxies for the oxidation state of magmas[J]. *Geochimica et Cosmochimica Acta*, 97: 70–87.
- Wang B, Shu L S, Faure M, et al. 2011. Paleozoic tectonics of the southern Chinese Tianshan: Insights from structural, chronological and geochemical studies of the Heiyingshan ophiolitic mélange (NW China)[J]. *Tectonophysics*, 497(1/4): 85–104.
- Wang B, Shu L S, Faure M, et al. 2013. Tectonic evolution of Tarim active continental margin and Southern Tianshan in Early Paleozoic[J]. *Acta Geological Sinica*, 87(S1): 82–83 (in Chinese with English abstract).
- Wang B, Song F, Ni X H. 2022. Paleozoic accretionary orogenesis and major transitional tectonic events of the Tianshan orogen[J]. *Acta Geological Sinica*, 96(10): 3514–3540 (in Chinese with English abstract).
- Wang B, Zhai Y Z, Kapp P, et al. 2018b. Accretionary tectonics of back-arc oceanic basins in the South Tianshan: insights from structural, geochronological and geochemical studies of the Wuwamen ophiolite mélange[J]. *GSA Bulletin*, 130(1/2): 284–306.
- Wang M, Zhou H R, Zhang H. 2019. Detrital zircon geochronology and tectonic implications of the Mesoproterozoic Gaoshanhe Group in south margin of North China Craton[J]. *Journal of Palaeogeography*, 22(1): 39–55 (in Chinese with English abstract).
- Wang X S, Klemd R, Gao J, et al. 2018a. Final assembly of the southwestern Central Asian Orogenic Belt as constrained by the evolution of the South Tianshan Orogen: Links with Gondwana and Pangea[J]. *Journal of Geophysical Research: Solid Earth*, 123: 7361–7388.
- Watson E B, Harrison T M. 2005. Zircon thermometer reveals minimum melting conditions on concreted earth[J]. *Science*, 308(5723): 841–844.
- Windley B F, Alexeiev D, Xiao W J, et al. 2007. Tectonic models for accretion of the Central Asian Orogenic Belt[J]. *Journal of the Geological Society*, 164(1): 31–47.
- Wu F Y, Li X H, Yang J H, et al. 2007. Discussions on the petrogenesis of granites[J]. *Acta Petrological Sinica*, 23(6): 1217–1238 (in Chinese with English abstract).
- Wu F Y, Yang J H, Liu X M, et al. 2005. Hf isotopic characteristics of 3.8 Ga zircon from eastern Hebei Province and the early crustal age of North China Craton[J]. *Chinese Science Bulletin*, 50(18): 1996–2003 (in Chinese with English abstract).
- Wu Y B, Zheng Y F. 2004. Genetic mineralogy of zircon and its restriction on U–Pb age interpretation[J]. *Chinese Science Bulletin*, 49(16): 1589–1604 (in Chinese with English abstract).
- Xiao W J, Santosh M. 2014. The western Central Asian Orogenic Belt: A window to accretionary orogenesis and continental growth[J]. *Gondwana Research*, 25(4): 1429–1444.
- Xiao W J, Windley B F, Sun S, et al. 2015. A tale of amalgamation of three Permo-Triassic collage systems in Central Asia: Oroclines, sutures, and terminal accretion[J]. *Annual Review of Earth and Planetary Sciences*, 43(1): 477–507.
- Xiao W J, Windley B F, Yuan C, et al. 2009. Paleozoic multiple subduction–accretion processes of the southern Altaids[J]. *American Journal of Science*, 309(3): 221–270.
- Yan L L, He Z Y, Beier C, et al. 2018. Zircon trace element constrains on the link between volcanism and plutonism in SE China[J]. *Lithos*, 320/321: 28–34.
- Yan L L, He Z Y, Klemd R, et al. 2020. Tracking crystal–melt segregation and magma recharge using zircon trace element data[J]. *Chemical Geology*, 542: 119596.
- Yang J H, Cawood P A, Du Y S, et al. 2012. Large Igneous Province and magmatic arc sourced Permian–Triassic volcanogenic sediments in China[J]. *Sedimentary Geology*, 261/262: 120–131.
- Yang J S, Xu X Z, Li T F, et al. 2010. U–Pb ages of zircons from ophiolite and related rocks in the Kumishi region at the southern margin of Middle Tianshan, Xinjiang: Evidence of Early Paleozoic oceanic basin[J]. *Acta Petrological Sinica*, 27(1): 77–95 (in Chinese with English abstract).
- Yang S H, Zhou M F. 2009. Geochemistry of the similar to 430 Ma Jingbulake mafic–ultramafic intrusion in Western Xinjiang, NW China: Implications for subduction related magmatism in the South Tianshan orogenic belt[J]. *Lithos*, 113(1): 259–273.
- Yu X H, Qin Q, Huang H, et al. 2020. Genesis and tectonic significance of the Mangqisu pluton in the South Tianshan; evidence from geochronology, geochemistry, and Nd–Hf isotopes[J]. *Acta Geological Sinica*, 94(10): 2893–2918 (in Chinese with English abstract).

Zhao Z Y, Zhang Z C, Santosh M, et al. 2015. Early Paleozoic magmatic— record from the northern margin of the Tarim Craton: Further insights on the evolution of the Central Asian orogenic belt [J]. *Gondwana Research*, 28(1): 328–347.

Zhou A R G L, Dai J G, Li Y L, et al. 2017. Zircon trace element geochemical characteristics of Late Silurian–Early Jurassic granitoids from Eastern Kunlun Range and its geological significance [J]. *Acta Petrological Sinica*, 33(1): 173–190 (in Chinese with English abstract).

Zhu Z X, Li J Y, Dong L H, et al. 2008. The age determination of Late Carboniferous intrusions in Mangqisu region and its constraints to the closure of oceanic basin in South Tianshan, Xinjiang [J]. *Acta Petrological Sinica*, 24(12): 2761–2766 (in Chinese with English abstract).

附中文参考文献

高俊, 钱青, 龙灵利, 等. 2009. 西天山的增生造山过程 [J]. *地质通报*, 28(12): 1804–1816.

郭瑞清, 秦切, 木合塔尔, 等. 2013. 新疆库鲁克塔格西段奥陶纪花岗岩体地质特征及构造意义 [J]. *地学前缘*, 20(4): 251–263.

黄永高, 罗改, 张彤, 等. 2019. 滇西丽江小桥头岩体时代与成因: 锆石 U–Pb 定年与微量元素证据 [J]. *桂林理工大学学报*, 39(1): 26–37.

雷玮琰, 施光海, 刘迎新. 2013. 不同成因锆石的微量元素特征研究进展 [J]. *地学前缘*, 20(4): 273–284.

李同宇, 金超, 田忠华, 等. 2022. 乳山地区中生代花岗岩及捕虏体年代学、Hf 同位素特征对胶东半岛地壳演化的启示 [J]. *地球科学*, 47(8): 2951–2967.

李曰俊, 杨海军, 赵岩, 等. 2009. 南天山区域大地构造与演化 [J]. *大地构造与成矿学*, 33(1): 94–104.

李壮, 李兴怡, 张鹏, 等. 2022. 西藏浦桑果矿区中新世中酸性侵入岩锆石微量元素特征及地质意义 [J]. *地质论评*, 68(4): 1236–1260.

刘桂萍, 郭瑞清, 蔡宏明, 等. 2020. 新疆南天山克孜尔河沉积物碎屑锆石 U–Pb 年代学研究及其地质意义 [J]. *地质科学*, 56(1): 210–236.

刘桂萍. 2021. 南天山造山带古生代地壳生长与演化——来自现代河流碎屑锆石年代学及 Hf 同位素的约束 [D]. 中国矿业大学博士学位论文.

王博, 舒良树, Faure M, 等. 2013. 塔里木早古生代活动陆缘与南天山构造演化 [J]. *地质学报*, 87(S1): 82–83.

王博, 宋芳, 倪兴华, 等. 2022. 天山古生代增生造山作用及其构造转换事件 [J]. *地质学报*, 96(10): 3514–3540.

王森, 周洪瑞, 张恒. 2019. 华北南缘中元古界高山河群碎屑锆石 U–Pb 年代学及其地质意义 [J]. *古地理学报*, 22(1): 39–55.

吴福元, 李献华, 杨进辉, 等. 2007. 花岗岩成因研究的若干问题 [J]. *岩石学报*, 23(6): 1217–1238.

吴福元, 杨进辉, 柳小明, 等. 2005. 冀东 3.8 Ga 锆石 Hf 同位素特征与华北克拉通早期地壳时代 [J]. *科学通报*, 50(18): 1996–2003.

吴元保, 郑永飞. 2004. 锆石成因矿物学研究及其对 U–Pb 年龄解释的制约 [J]. *科学通报*, 49(16): 1589–1604.

新疆维吾尔自治区地质矿产局. 1993. 新疆维吾尔自治区区域地质志 [M]. 北京: 地质出版社.

新疆维吾尔族自治区地质局. 1959. 1 : 20 万库尔勒幅地图 [R].

杨经绥, 徐向珍, 李天福, 等. 2010. 新疆中天山南缘库米什地区蛇绿岩的锆石 U–Pb 同位素定年: 早古生代洋盆的证据 [J]. *岩石学报*, 27(1): 77–95.

于新慧, 秦切, 黄河, 等. 2020. 南天山盲起苏花岗岩体的成因及构造意义: 来自年代学、地球化学及 Nd–Hf 同位素证据 [J]. *地质学报*, 94(10): 2893–2918.

周敖日格勒, 戴紧根, 李亚林, 等. 2017. 东昆仑山脉晚志留世—早侏罗世花岗类岩石中锆石微量元素地球化学特征及地质意义 [J]. *岩石学报*, 33(1): 173–190.

朱志新, 李锦轶, 董连慧, 等. 2008. 新疆南天山盲起苏晚石炭世侵入岩的确定及对南天山洋盆闭合时限的限定 [J]. *岩石学报*, 24(12): 2761–2766.